ACS Catalysis

Research Article

pubs.acs.org/acscatalysis

Catalytic Hydrogenation of CO_2 to Formates by a Lutidine-Derived Ru−CNC Pincer Complex: Theoretical Insight into the Unrealized Potential

Georgy A. Filonenko,[†,‡,⊥] Daniel Smykowski,[†,§,⊥] Bartłomiej M. Szyja,[∥] Guanna Li,[†] Jerzy Szczygieł,[§] Emiel J. M. Hensen,[†,‡] and Evgeny A. Pidko*[,†,‡]

[†]Inorganic Materials Chemistry Group, Schuit Institute of Catalysis, and [‡]Institute for Complex Molecular Systems, Eindhoven University of Technology, P.O. Box 513, 5600 MB Eindhoven, The Netherlands

[§]Department of Chemistry, Wrocław University of Technology, Gdańska 7/9, 50-344 Wrocław, Poland

[∥]Institute for Solid State Theory, Westfälische Wilhelms-Universität Münster, Wilhelm Klemm Straße 10, 48149 Münster, Germany

Supporting Information

ABSTRACT: Metal−ligand cooperative properties of a bis-N-heterocyclic carbene ruthenium CNC pincer catalyst and its activity in CO_2 hydrogenation to formates were studied by DFT calculations complemented by NMR spectroscopy and kinetic measurements. The dearomatized Ru−CNC* pincer (**1***) is significantly more reactive toward metal−ligand cooperative activation of H_2 and CO_2 than the structurally related phosphine-based Ru−PNP complex. The enhanced reactivity of Ru−CNC* stems from the combination of electronic properties of this system and the reduced geometric constraints imposed onto the Ru center by the large and flexible CNC chelate. Heterolytic dissociation of H_2 by **1*** results in the bis-hydrido complex **2** that is active in hydrogenation of CO_2. However, under commonly applied reaction conditions, the catalyst rapidly deactivates via metal−ligand cooperative paths. The transient formation of the dearomatized complex Ru−CNC* (**1***) in the course of the reaction leads to the irreversible cooperative activation of CO_2, resulting in the stable adduct **3** that is not catalytically competent. By an increase in the H_2/CO_2 ratio, this deactivation path can be effectively suppressed, resulting in a stable and rather high catalytic performance of Ru−CNC.

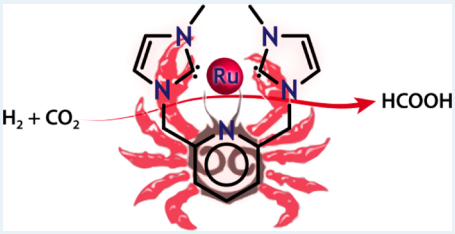

KEYWORDS: *DFT calculations, ruthenium, N-heterocyclic carbene, hydrogenation, catalyst deactivation, metal−ligand cooperation*

INTRODUCTION

The development of technologies that will enable efficient utilization of carbon dioxide in chemical synthesis represents a major challenge to catalysis scientists working in industry and academia. A variety of catalytic pathways that make use of heterogeneous[1] and homogeneous[2] catalysts for CO_2 conversion have been discussed. Homogeneous catalysis approaches often make use of the rich CO_2 coupling chemistry for the synthesis of value-added products. In the last few years, significant progress has been made in catalytic coupling of CO_2 with alkenes,[3] alkynes,[4] and epoxides.[5] An alternative to CO_2 coupling reactions is its hydrogenation to methanol[6] or formic acid (FA). Both products are fuels and also serve as important intermediates in chemical synthesis. In recent years, FA has attracted renewed[7] attention as a potential hydrogen carrier.[8] The catalytic decomposition of FA produces CO-free hydrogen, which can be directly used in fuel cells.[9] Efficient production of FA by catalytic hydrogenation of CO_2 would pave the way toward cleaner energy technologies.[8,9b,10]

Formic acid is produced industrially from methyl formate generated by carbonylation of methanol.[11] The major obstacle for direct FA production from CO_2 is the unfavorable reaction thermodynamics. This, however, can be circumvented by using a base promoter that in situ neutralizes FA and, thereby, shifts the reaction equilibrium toward the formate salt product.[12]

Last year, the field of catalytic hydrogenation of carbon dioxide to formates celebrated its 100th anniversary. The first catalytic system based on Pd black was described by Bredic and Carter in 1914.[13] In spite of the long history of this reaction,[7,14] significant progress has only been witnessed in the last few decades.[15] Recent studies provide several examples of efficient catalysis with non-noble transition-metal complexes.[16] However, the highest catalytic activities have been achieved with homogeneous catalysts based on noble metals[17] such as Rh,[18] Ir,[19] and Ru.[20] A particularly active system based on an Ir-PNP pincer complex was disclosed by Nozaki and co-workers in 2009.[19b] It allowed CO_2 hydrogenation rates up to 150000 h^{-1} at 200 °C. An important feature of the Ir−PNP catalyst is the "non-innocent" behavior of the lutidine-derived PNP pincer ligand. It can undergo chemical transformations to assist the transition metal in activating substrates. In the presence of a strong base, the deprotonation of the ligand yields a dearomatized complex, in which the reactive five-coordinated

Received: November 3, 2014
Published: January 9, 2015

DOI: 10.1021/cs501990c
ACS Catal. 2015, 5, 1145−1154

metal center is adjacent to a base site on the side arm of the pincer ligand (see Scheme 1 for examples). Cooperation

Scheme 1. Representative Lutidine-Derived Ru−Pincer Complexes and Their Metal−Ligand Cooperative Behavior toward Strong Bases, CO_2, and H_2

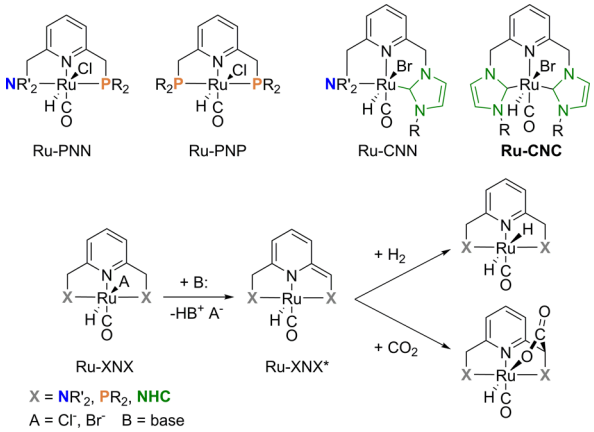

between the metal and the ligand (metal−ligand cooperation, MLC) is often invoked to explain the unique catalytic properties of this class of homogeneous catalysts.[21] For example, in the case of Nozaki's Ir−PNP, the ligand-assisted H_2 activation by dearomatized species has been argued to be one of the key steps in the catalytic cycle of CO_2 hydrogenation.[19c]

Related ruthenium-based pincers also show a good performance in CO_2 activation. Milstein and co-workers demonstrated that a lutidine-derived Ru−PNP catalyst, after being dearomatized by reaction with a strong base, can cooperatively add dihydrogen[22] and carbon dioxide[23] (Scheme 1). The cooperative addition of CO_2 across the metal and the ligand in a transition-metal pincer complex represents a new way of activating CO_2. Similar reactivity has been demonstrated for a Ru−PNN catalyst.[24] We have recently studied the impact of such MLC paths on the activity of Ru−PNP in CO_2 hydrogenation.[25] It was shown that the heterolytic H_2 dissociation by the dearomatized Ru−PNP* leads to the catalytically superior bis-hydrido Ru species, whereas the [1,3]-addition of CO_2 results in a pronounced inhibition of the catalyst performance. Because the former path is thermodynamically preferred for Ru−PNP, a substantial concentration of the reactive bis-hydrido complexes will be present under reaction conditions, resulting in good catalytic performance.[25] As a result, Ru−PNP catalyst in combination with the strong non-nucleophilic DBU base allows for unprecedented reaction rates (initial turnover frequency, TOF) of up to 1892000 h^{-1} at 132 °C,[26] which remains the highest activity reported to date for catalytic hydrogenation of CO_2 to formates.

Homogeneous catalysts involving N-heterocyclic carbenes (NHC) as donors offer several advantages over the phosphine-based systems.[27] In addition to being inherently stronger donor ligands, their steric and electronic properties can be easily varied by employing the well-established chemistry of heterocyclic compounds. Recently, several ruthenium complexes bearing cooperative lutidine-derived CNN[28] and CNC[29] ligands have been described. They show pronounced reactivity toward ligand dearomatization and cooperative activation of dihydrogen (Scheme 1). However, the catalytic activity of bis-NHC Ru−CNC pincer complexes described recently by us[29b] in CO_2 hydrogenation is strikingly low in comparison to the outstanding performance of the structurally related Ru−PNP system.[26] The origin of this difference is moot.

In this work, we employ density functional theory (DFT) calculations complemented by in situ NMR spectroscopy and kinetic experiments to get an insight into the mechanism of CO_2 hydrogenation by a representative Ru−CNC pincer catalyst and identify potential routes for the improvement of the catalytic activity of this new hydrogenation catalyst platform. The first part of the paper is devoted to the theoretical analysis of the cooperative behavior of the dearomatized Ru−CNC* complex **1*** toward H_2 and CO_2 activation, followed by a discussion of the DFT results on the possible chemical transformations underlying the catalytic properties of Ru−CNC in CO_2 hydrogenation. Both cooperative (MLC) and noncooperative (hydrogenolysis) paths for the catalytic reaction by the bis-hydrido Ru−CNC catalyst **2** are considered (Scheme 2).[26] The catalytic role of the

Scheme 2. Possible Catalytic Cycles for CO_2 Hydrogenation to Formates by Ru−CNC Pincer Catalysts[a]

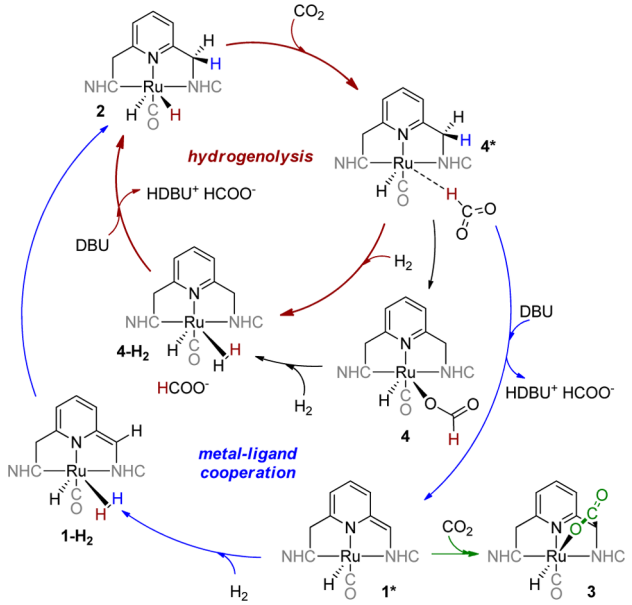

[a]imidazol-2-ylidene donors at the pincer arm are denoted as NHC

cooperative [1,4]-CO_2 adduct **3** is also evaluated. A direct comparison with the structurally related Ru−PNP catalyst is presented. The computational predictions are then verified by NMR experiments and catalytic tests.

COMPUTATIONAL AND EXPERIMENTAL DETAILS

Density Functional Theory Calculations. The computational methodology employed in our previous studies[25,26] on the catalytic properties of the related Ru−PNP pincer system was used in this work. All DFT calculations were carried out using the hybrid PBE0[30] exchange-correlation functional as implemented in the Gaussian 09 D.01 program.[31] Previous benchmark studies evidenced the high accuracy of this method for the description of a wide range of chemical systems.[33] The all-electron 6-311G(d,p) basis set was used for all atoms except ruthenium, for which the LanL2DZ basis set was employed. The polarized continuum model (PCM) was employed during

DOI: 10.1021/cs501990c
ACS Catal. 2015, 5, 1145−1154

geometry optimization and frequency analysis to account for bulk solvent effects. All complexes were treated as neutral species. Previously, we showed[26] that a perfect agreement between the experimental and computationally predicted geometries of Ru pincer complexes and reaction thermodynamics can be achieved by using this approach. Furthermore, the accuracy of the selected methodology has been confirmed by computing the energetics of selected elementary steps of CO_2 hydrogenation by Ru−PNP using a larger triple-ζ + polarization quality basis set combination employing the Def2-TZVPP basis set for the Ru center and 6-311+G(d,p) for other atoms.[25,26] The impact of weak van der Waals interactions on the reaction energetics was evaluated by performing additional single-point calculations on the Ru−CNC intermediates involved in **1***-H_2 → **2** and **1***-CO_2 → **3** transformations using the PBE0-D3 method as implemented in Gaussian 09 D.01 in combination with the high-level triple-ζ + polarization quality basis set. The energetics computed using these higher-level methodologies agreed within 6 kJ mol^{-1} with those obtained using the standard procedure.

The nature of the stationary points was evaluated from the analytically computed harmonic modes. No imaginary frequencies were found for the optimized structures, while all transition states exhibited a single imaginary frequency, corresponding to the eigenvector along the reaction path. The assignment of the transition state structure to a particular reaction path was tested by perturbing the structure along the reaction path eigenvector in the directions of the product and the reagent followed by geometry optimization. The reaction (ΔE_{ZPE}) and activation energies ($E_{ZPE}^{\ddagger}$) reported in the paper were corrected for zero-point energy contribution computed using the results of the normal-mode analysis. Reaction Gibbs free energies (ΔG°) and activation Gibbs free energies ($G^{\circ,\ddagger}$) were computed using the results of the normal-mode analysis within the ideal gas approximation at a pressure of 1 atm and temperature of 298 K. Further computational details can be found in ref 26.

The effect of the composition of the reaction mixture on the relative stability of Ru−CNC complexes under the catalytic conditions was evaluated by using the ab initio thermodynamic analysis method. Individual Gibbs free energy profiles at varying partial pressures of H_2 and CO_2 were constructed on the basis of the DFT-computed energies and temperature-dependent entropy and internal thermal energy contributions of gaseous H_2 and CO_2 components. The overall reactions associated with the individual catalytic cycles shown in Scheme 2 were used to compute the thermodynamic parameters. The dearomatized Ru−CNC* complex **1*** was chosen as the reference state. For more details see ref 32 and the Supporting Information.

In Situ NMR and Kinetic Study on Catalytic CO_2 Hydrogenation. All manipulations, unless otherwise stated, were performed using Schlenk techniques. Argon was dried with a Sicapent column. Air-sensitive compounds were stored in an MBraun glovebox under an atmosphere of dry nitrogen or argon. Solvents were dispensed from an MBraun solvent purification system. 1,8-Diazabicyclo[5.4.0]undec-7-ene (DBU) was purchased from Fluorochem and vacuum-distilled from calcium hydride. The pure bromide form of Ru−CNC pincer **1** was prepared according to the original procedure involving the reaction of the mesityl-substituted bis-imidazolium bromide ligand, the base 2-*tert*-butylimino-2-diethylamino-1,3-dimethyl-perhydro-1,3,2-diazaphosphorine (BEMP), and RuHCl(CO)-$(PPh_3)_3$ precursor in THF in the presence of LiBr.[29b]

The high-pressure in situ NMR studies were carried out using a heavy-wall Wilmad Quick pressure NMR tube. Deuterated DMF was purchased from Eurisotop and dried over molecular sieves, degassed, and stored over freshly activated molecular sieves. NMR spectra were recorded on Varian Mercury 400 MHz and Varian Inova 500 MHz spectrometers. Chemical shifts were referenced to residual solvent peaks.

Kinetic measurements were carried out in a Top Industrie 100 mL stainless steel autoclave. Prior to the reaction the vessel was evacuated overnight at 150 °C and purged several times with Ar. The reaction medium was introduced by cannula transfer. The autoclave was flushed with H_2, preheated to the reaction temperature, and filled with an H_2/CO_2 mixture up to an operating pressure of 40 bar. The catalyst was then introduced via a dosage device and the reaction was started. Constant pressure was maintained by a compensation device fitted with a Bronkhorst EL-FLOW MFC unit and digital pressure meter with an equimolar H_2/CO_2 mixture to ensure the continuous reactant supply. The stirring rate was maintained at 1000 rpm to ensure an efficient gas/liquid mass transfer.[26] Samples were withdrawn via a dip-tube installation (dead volume 4 μL, sampling volume 110 μL), diluted to 1 mL, and immediately analyzed by HPLC and GC-FID. In a typical experiment, 30 mL of DMF, 5 mL of DBU (33.4 mmol), 1 mL of toluene or THF (used as an internal standard), and an appropriate amount of catalyst dispensed from the stock solution were used. A more detailed description of employed procedures and techniques can be found in ref 26.

RESULTS AND DISCUSSION

Metal−Ligand Cooperation. The catalytic activity of lutidine-derived hydrogenation Ru catalysts is usually triggered by reaction with a strong base, resulting in ligand dearomatization and a concomitant elimination of one of the anionic ligands (Scheme 1). The cooperative action of the thus formed basic CH moiety (C*) at the pincer arm and the five-coordinated Ru center toward substrate activation is considered to be one of the key properties of this class of homogeneous catalysts.

Because of the highly nonplanar geometry of the chelate in Ru−CNC and its substantial lateral flexibility, the initial deprotonation step can yield the two nonequivalent stereoisomers **1*** and **1a*** (Scheme 3), depending on the relative orientation of the leaving groups in **1**. The stereoisomers **1** and **1a** are characterized by identical main geometrical parameters and similar stabilities (Figure 1). They correspond to atropisomers, as they can interconvert via a frustrated rotation of the methylene bridge with an activation barrier ($E_{ZPE}^{\ddagger}$) of only 66 kJ mol^{-1} and activation Gibbs free energy barrier ($G^{\circ,\ddagger}_{ZPE}$) of 70 kJ mol^{-1}. Such a low barrier of internal rotation implies their fast equilibration at relatively low temperatures.[34]

Despite similar geometries (e.g., r(Ru···C*) = 3.416 Å in **1** and 3.420 Å in **1a***), these complexes are expected to exhibit substantially different acid−base cooperative properties because of the different spatial orientations of the reactive Ru and C* sites (schematically depicted with red and blue stars in Scheme 3). Indeed, whereas the empty d_{z^2} orbital of the metal and the p_{C^*} lone pair on C* are coaligned in **1***, they point in different directions in **1a***. Consequently, the cooperative activation of H_2 toward a rearomatized bis-hydrido complex **2** can be promoted only by **1*** (Scheme 3),[29b] in which the direct cooperation between Ru and C* centers promotes the

DOI: 10.1021/cs501990c
ACS Catal. 2015, 5, 1145−1154

Scheme 3. Acid–Base Metal–Ligand Cooperative Activation of H_2 and CO_2 by Deprotonated Ru–CNC Complexes

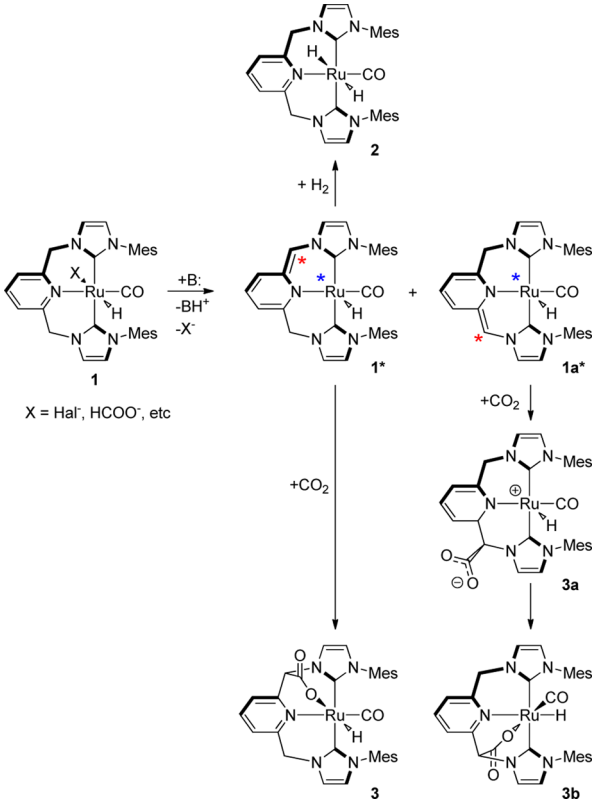

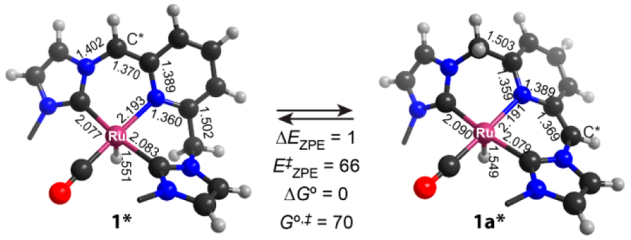

Figure 1. Optimized structures of atropisomers **1*** and **1a*** and DFT-computed energetics of their interconversion (in kJ mol^{-1}). Selected interatomic distances are given in Å. Mes substituents at the NHC moieties are omitted for clarity.

heterolytic dissociation of H_2. The respective DFT results are summarized in Figure 2. The reaction starts with the slightly endergonic (ΔG° = 15 kJ mol^{-1}) coordination of H_2 to **1***, resulting in the σ complex **1-H$_2$** characterized by symmetric η^2 coordination of an elongated H_2 molecule (r(H–H) = 0.809 Å in comparison to the value of 0.747 Å computed for the free molecule at the same level of theory). Next, the precoordinated H_2 dissociates heterolytically to yield complex **2** (ΔE_{ZPE} = −56 kJ mol^{-1}, $E^{\ddagger}_{ZPE}$ = 15 kJ mol^{-1}). Similar to the analogous reaction with the Ru–PNP* system,[26] the entropy contributions in this case are negligible because of the immobilization of H_2 in the σ complex.

By analogy with Ru–PNP, DFT calculations predict that **1*** can promote the cooperative [1,4]-addition of CO_2 (**1*** + CO_2 → **3**, Scheme 3 and Figure 3). The formation of the nonspecific molecular complex **1-CO$_2$** is followed by a barrierless and highly exothermic (ΔE_{ZPE} = −119 kJ mol^{-1}; $E^{\ddagger}_{ZPE}$ = 1 kJ mol^{-1}) insertion of CO_2, resulting in **3**. Because the initial CO_2

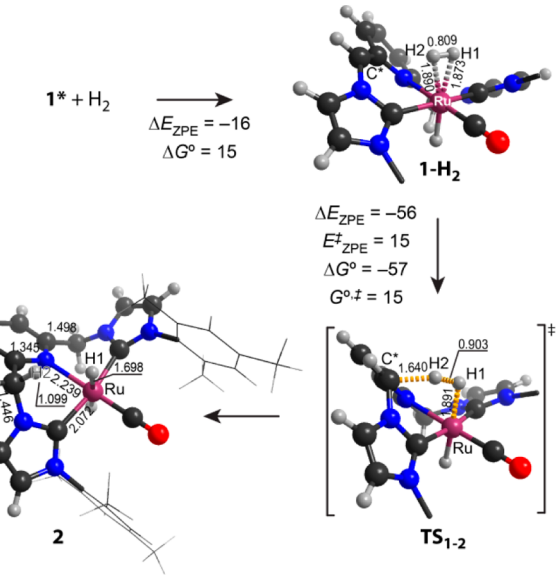

Figure 2. Optimized structures of reaction intermediates and transition state of a metal–ligand cooperative H_2 activation by **1** (Mes substituents at the NHC moieties are omitted for clarity).

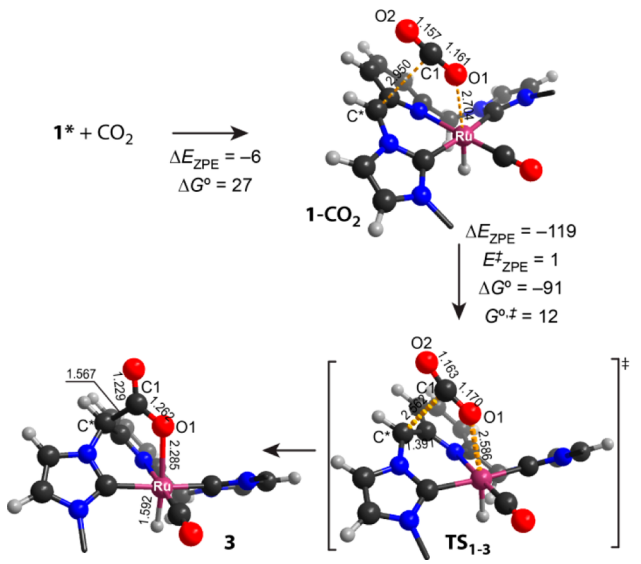

Figure 3. Optimized structures of intermediates and transition state of a [1,4]-addition of CO_2 to **1*** (Mes substituents at the NHC moieties are omitted for clarity).

coordination is endergonic, the overall free energy barrier ($G^{\circ,\ddagger}$) of the reaction is 39 kJ mol^{-1}, which is 9 kJ mol^{-1} higher than the value predicted for the H_2 dissociation by **1*** (**1*** + H_2 → **2**). The reaction proceeds via the early transition state **TS$_{1\text{-}3}$**, as can be seen from the very small structural perturbations of the reactive species involved in the TS. In line with our earlier proposal,[26] this implies that the [1,4]-addition of CO_2 to **1*** is triggered by the attack of the bent CO_2 molecule by the basic C* site. The coordination with Ru provides an additional stabilization of the CO_2 adduct. This interaction is particularly effective in **3**, due to the specific geometric properties of the CNC ligand. Its structure features a Ru···O1 bond (2.285 Å) shorter than that in the related Ru–PNP [1,3]-CO_2 adduct (r(Ru···O1)$_{PNP}$ = 2.319 Å).[26] Furthermore, the larger CNC chelate imposes less constraint onto the quite rigid tetradentate

DOI: 10.1021/cs501990c
ACS Catal. 2015, 5, 1145–1154

ligand geometry in **3** (Figure 3). This provides a plausible explanation for an almost two-fold higher exothermicity of the CO_2-addition reaction to Ru−CNC* (**1*** + CO_2 → **3**, ΔE_{ZPE} = −125 kJ mol^{-1}) in comparison to that predicted for Ru−PNP* (ΔE_{ZPE} = −61 kJ mol^{-1}).[26]

Following the above proposition on the key role of the basic ligand site for CO_2 activation, we also considered computationally a noncooperative mechanism of CO_2 addition to **1a*** (**1a*** + CO_2 → **3a** → **3b**; Scheme 3 and Figure 4). The initial

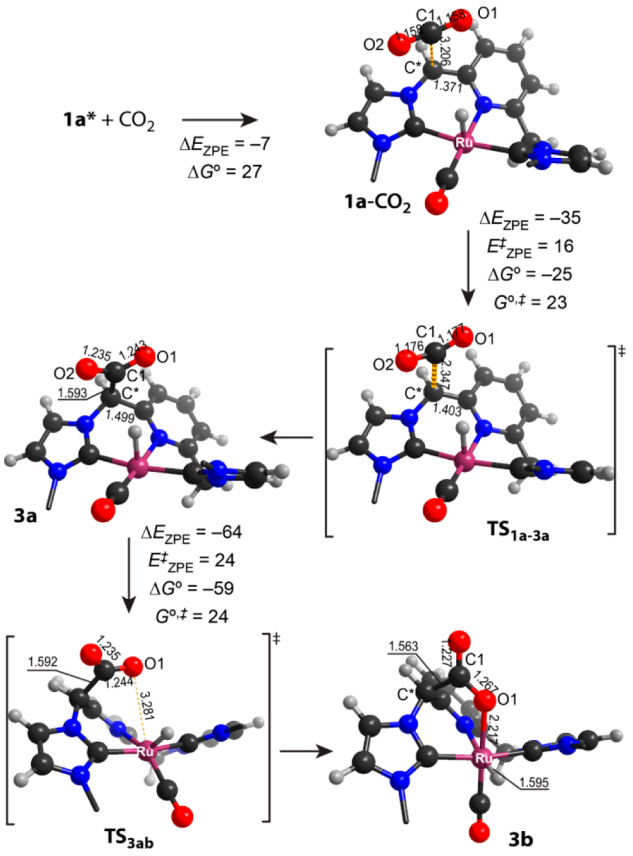

Figure 4. Optimized structures of intermediates and transition state of a noncooperative addition of CO_2 to **1a*** (Mes substituents at the NHC moieties are omitted for clarity).

molecular complexes for the cooperative (**1-CO$_2$**, Figure 3) and noncooperative (**1a-CO$_2$**, Figure 4) CO_2 addition paths show similar binding energies, despite the lack of additional Ru···O coordination in the latter structure. The reaction of CO_2 with **1a*** leads to the metastable intermediate **3a**, containing a noncoordinated carboxylate moiety at the pincer arm. The five-coordinated state of Ru is preserved upon CO_2 addition. This step is thermodynamically favored and proceeds with an activation barrier of only 16 kJ mol^{-1} (Figure 4). The relatively low stability of **3a** is associated with its zwitterionic nature. The system can be further stabilized via a reorganization of the ligand environment, resulting in complex **3b** (ΔE_{ZPE} = −64 kJ mol^{-1}; Figure 4). The rotation of the carboxylate moiety around the C*−C1 bond displaces the axial hydride ligand into the equatorial position with a concomitant change in the configuration of the CO ligand and the formation of a Ru−O1 coordination bond (**3a** → **TS$_{3ab}$** → **3b**; Figure 4). The overall barrier for the noncooperative CO_2 addition (**1a*** + CO_2 → **3b**, $G^{o,\ddagger}_{app}$ = 50 kJ mol^{-1}, ΔG° = −57 kJ mol^{-1}) is only 11 kJ mol^{-1} higher than that for the metal−ligand cooperative path (**1*** + CO_2 → **3**, $G^{o,\ddagger}_{app}$ = 39 kJ mol^{-1}, ΔG° = −75 kJ mol^{-1}), while it is much lower than the free energy barrier for the isomerization of **1*** and **1a*** ($G^{o,\ddagger}_{app}$ = 70 kJ mol^{-1}).

Alternative paths for H_2 and CO_2 activation by **1*** involving the rearrangement of the CNC chelate into the facial coordination mode[29a] are very unfavorable (Figure S1, Supporting Information). For example, heterolytic H_2 dissociation by **1*** yielding a facial stereoisomer of the bis-hydrido Ru−CNC complex (*fac*-**2**) is thermodynamically unfavorable (**1*** + H_2 → *fac*-**2**, ΔG° = 21 kJ mol^{-1}) and proceeds with a very high overall free energy barrier ($G^{o,\ddagger}_{app}$ = 122 kJ mol^{-1}).

The results presented so far indicate that both the heterolytic H_2 dissociation and CO_2 addition to **1*** are thermodynamically and kinetically more favorable than the corresponding reactions with the dearomatized Ru−PNP* complex. These reactivity differences can be partially rationalized by comparing the frontier orbitals of these complexes (Figure 5). For both systems, an unoccupied d_{z^2} orbital on Ru and an occupied formally p_z orbital on C1* are the largest contributors to the LUMO and HOMO, respectively. An occupied d_{yz} orbital on Ru represents HOMO-1. The higher basicity of the C* site in

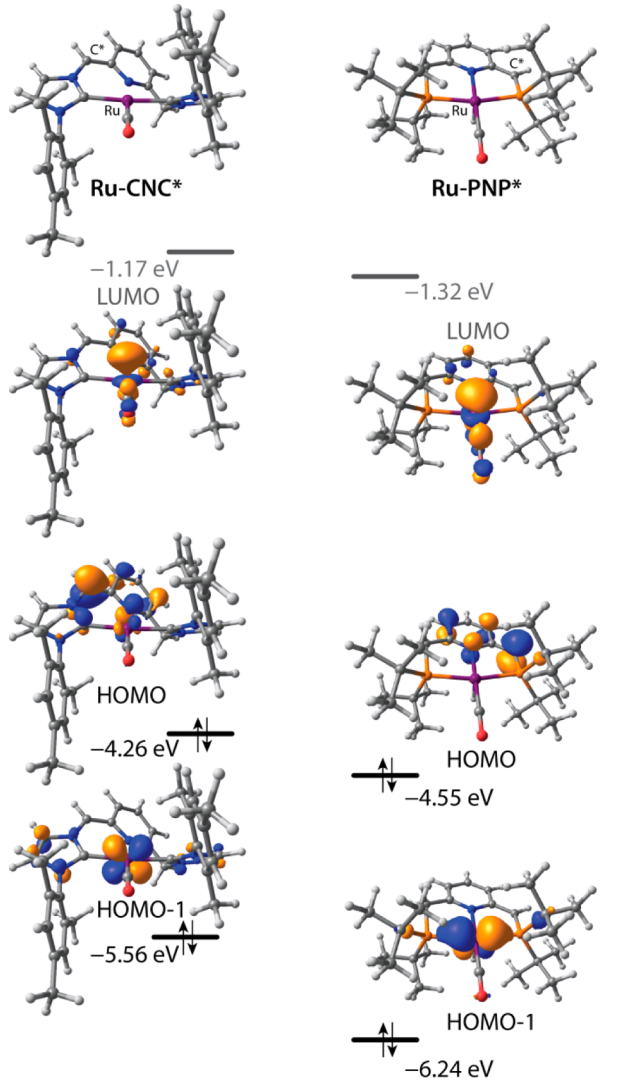

Figure 5. Comparison of frontier orbitals of the dearomatized Ru−CNC* complex **1*** and a related Ru−PNP* complex.

DOI: 10.1021/cs501990c
ACS Catal. 2015, 5, 1145−1154

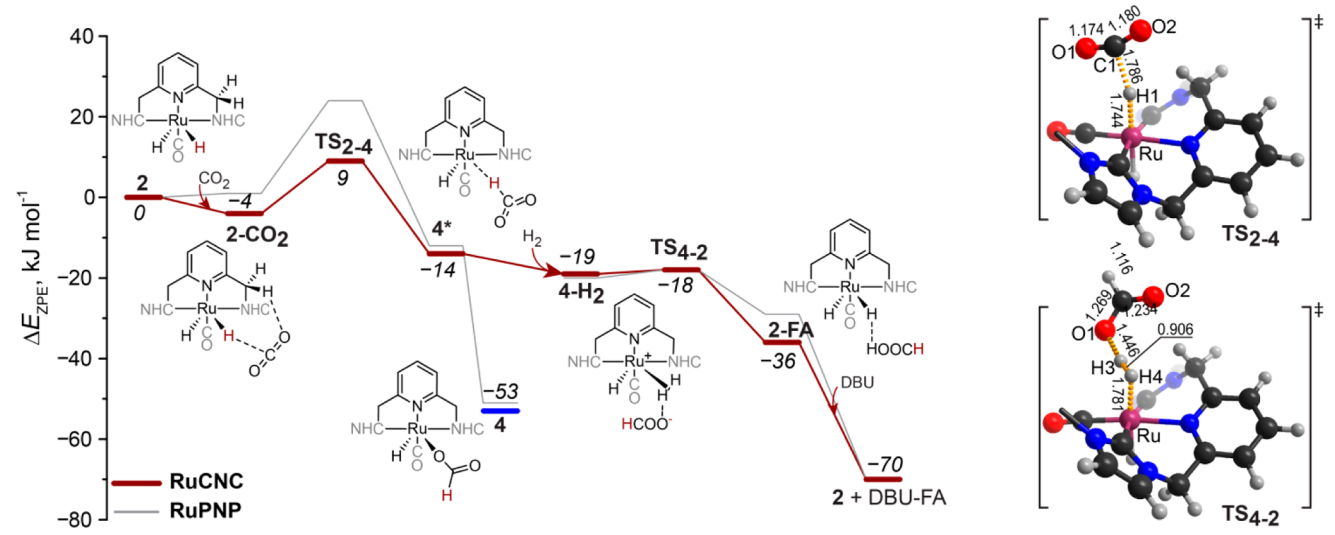

Figure 6. DFT-computed reaction energy diagram and optimized structures of the transition states involved in CO_2 hydrogenation by **2**. The respective energetics computed for the Ru−PNP analogue[25,26] is shown for comparison.

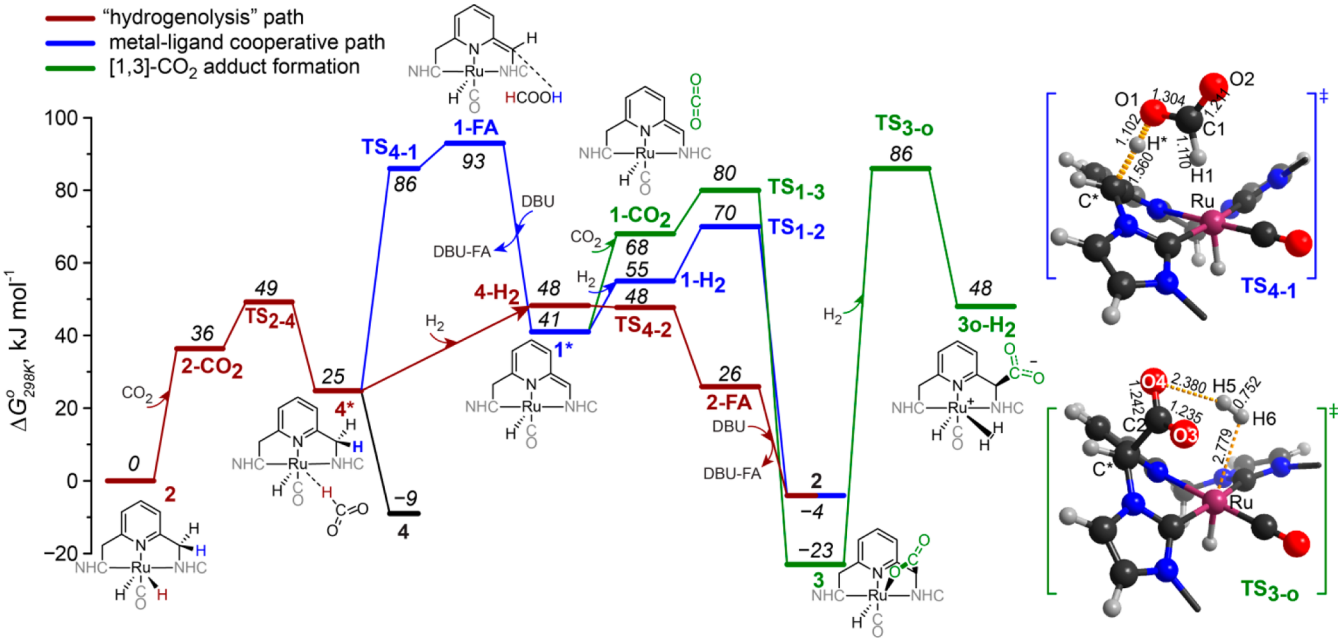

Figure 7. Comparison of Gibbs free energy diagrams for different reaction paths of CO_2 hydrogenation by Ru−CNC catalysts.

1* is evidenced by the substantially higher energy of the respective HOMO, which can form a more effective overlap with the LUMO of the hybridized bent CO_2 molecule, resulting in an enhanced acid−base interaction. This, together with the favorable geometry of the CNC chelate discussed above, determines the very low barrier and high exothermicity of the [1,4]-CO_2 addition to **1***.

Although the higher basicity of the pincer arm is also beneficial for the heterolytic cleavage of H_2 toward the bis-hydrido Ru complex **2**, the interaction with the Ru center is crucial in this case. In particular, H_2 dissociation is directly promoted by the back-donation from the d_{yz} orbital of Ru to the antibonding σ^* orbital of coordinated H_2. The enhanced reactivity of Ru−CNC* in H_2 dissociation is therefore contributed by the higher energy and the less diffuse character of the HOMO-1 orbital. The results in Figure 5 evidence a substantial contribution of P centers to the HOMO-1 of Ru−PNP. These rudimentary π-acceptor properties of the phosphine donors provide substantial stabilization of HOMO-1 in comparison to the case of pure σ-donating NHC groups in **1*** (Figure 5). Consequently, a more efficient back-donation is realized upon the interaction of H_2 with **1***. This strongly facilitates the H_2 dissociation by Ru−CNC* (**1-H$_2$** → **TS$_{1\text{-}2}$** → **2**, $E^{\ddagger}_{ZPE}$ = 15 kJ mol^{-1}, Figure 2) in comparison to the reaction with its phosphine-containing Ru−PNP* analogue ($E^{\ddagger}_{ZPE}$ = 75 kJ mol^{-1}).[26]

Summarizing, DFT calculations point to the much higher reactivity of the dearomatized Ru−CNC* complex toward the ligand-assisted activation of both H_2 and CO_2 in comparison to that of the Ru−PNP* system. Because of the pronounced atropoisomerism of Ru−CNC*, two alternative mechanisms of CO_2 addition can be realized, resulting in the distinctly different CO_2 adducts **3** and **3b**. Unlike in the case of Ru−PNP* where the reaction with H_2 resulting in the catalytically potent bis-

DOI: 10.1021/cs501990c
ACS Catal. 2015, 5, 1145−1154

hydrido complex is thermodynamically preferred, the cooperative addition of CO_2 to Ru−CNC* is more favorable. This exemplifies the crucial difference in the reactivity of Ru−PNP and Ru−CNC that adversely affects the catalytic application of the latter.

Catalytic Hydrogenation of CO_2. We further evaluated theoretically the intrinsic activity of the bis-hydrido complex **2** and the potential role of the CO_2 adduct **3** in catalytic CO_2 hydrogenation to formates. Figure 6 presents a DFT-computed reaction energy diagram for CO_2 hydrogenation, with **2** following the "hydrogenolysis" mechanism (Scheme 2). Calculated Gibbs free energy profiles for this cycle and for the competing paths involving complexes **1*** and **3** are compared in Figure 7.

The reaction starts with the slightly exothermic binding of CO_2 with **2**, resulting in **2-CO$_2$**. Under standard conditions, this step is endergonic (Figure 7). The polarization of coordinated CO_2 through the interaction with the acidic methylene protons facilitates the subsequent attack by the Ru-bound hydride (**TS$_{2\text{-}4}$**, Figure 6) that results in the non-coordinated formato complex **4*** (ΔE_{ZPE} = −10 kJ mol^{-1}, $E^{\ddagger}_{ZPE}$ = 13 kJ mol^{-1}). Under standard conditions, this initial CO_2 activation by **2** proceeds with an overall activation free energy barrier ($G^{\circ,\ddagger}_{app}$) of only 49 kJ mol^{-1} (Figure 7). This barrier is substantially lower than the barrier of 67 kJ mol^{-1} computed for Ru−PNP.[26] The difference is similar for the ZPE-corrected activation barriers (Figure 6), evidencing an intrinsically higher reactivity of Ru−CNC.

At the next step, the weakly coordinated $HCOO^-$ anion can be rapidly replaced with an H_2 molecule, resulting in the cationic σ complex **4-H$_2$** (**4*** + H_2 → **4-H$_2$**, ΔE_{ZPE} = −14 kJ mol^{-1}). The $HCOO^-$ anion in **4-H$_2$** forms rather short hydrogen bonds with both the dihydrogen ligand (r(O1···H3) = 2.232 Å) and the methylene bridge of the CNC ligand (r(O1···H2) = 2.084 Å). Shortening of the former bond results in heterolytic H_2 dissociation (**TS$_{4\text{-}2}$**; Figure 6) that yields a molecular complex of formic acid (FA) with **2** (**2-FA**). This step (**4-H$_2$** → **2-FA**) is thermodynamically favored and proceeds effectively without an activation barrier (Figures 6 and 7). A subsequent highly exothermic reaction with the DBU base eliminates the DBU-FA product and closes the catalytic cycle by regenerating the initial species **2**.

The contact ion pair **4*** can rearrange into the more stable formato complex **4** (ΔE_{ZPE} = −39 kJ mol^{-1}, ΔG° = −34 kJ mol^{-1}), which represents a resting state within the hydrogenolysis mechanism.[25] To proceed further with the catalytic reaction, the transformation of **4** to **4-H$_2$** is necessary. We were not able to identify a transition state for the one-step H_2 insertion reaction. Relaxed potential energy surface scans for the H_2 insertion pointed to effectively barrierless endothermic elimination of $HCOO^-$ from the coordination sphere of Ru in **4**, resulting in **4***, which can coordinate H_2. The cleavage of the HCOO−Ru coordination bond is promoted by the simultaneous formation of a short hydrogen bond between the formate anion and the methylene bridge.

This interaction of the weakly basic formate anion with the acidic methylene group in **4*** opens an MLC reaction path competitive with the main hydrogenolysis route. The endergonic barrierless transfer of an H* proton to O1 (**4*** → **TS$_{4\text{-}1}$** → **1*-FA**, Figure 7) followed by the immediate neutralization of the formed FA by DBU yields the DBU-FA adduct and the dearomatized complex **1***. The first deprotonation step determines the overall (free) energy barrier for this reaction (69 kJ mol^{-1}). The slightly endergonic formation of **1*** (ΔG° = 16 kJ mol^{-1}) is followed by a highly exothermic metal−ligand cooperative addition of either of the substrates via **1*** + CO_2 → **3**/**3b** or **1*** + H_2 → **2** transformations. The latter closes the catalytic cycle of the MLC mechanism. The irreversible reaction with CO_2 yields complex **3**, representing the most thermodynamically stable state among the species considered. Its transformation to potentially active species (**3** → **1*** + CO_2 or **3** + H_2 → **3°-H$_2$**) are strongly unfavorable thermodynamically and face free energy barriers exceeding 100 kJ mol^{-1} (Figure 7).

Experimental Validation and Performance Optimization. The computational results presented so far suggest that the intrinsic catalytic activity of the bis-hydrido Ru−CNC complex **2** is at least as high as that of the analogous Ru−PNP system. Both complexes can catalyze the conversion of CO_2 to formates via a hydrogenolysis route without involving metal−ligand cooperation. With excess H_2, a very low energy direct outer-sphere CO_2 activation path could have, in principle, been realized.[26] The respective catalytic cycle over **2** would involve a single and very small barrier of only 13 kJ mol^{-1} (**2-CO$_2$** → **TS$_{2\text{-}4}$** → **4***; Figure 6). We propose that the experimentally observed low catalytic activity of Ru−CNCs[29b] stems from the enhanced stability of the products of ligand-assisted CO_2 addition **3**/**3b**. DFT calculations suggest that, in the course of the catalytic reaction, the strong thermodynamic preference for the conversion of the reactive Ru complexes to CO_2 adducts will have a dramatic deteriorating effect on the overall catalytic performance.

To validate these theoretical predictions and get a further insight into the reactivity of Ru−CNC **1** under CO_2 hydrogenation conditions, an in situ NMR study has been carried out. In sharp contrast to the behavior of Ru−PNP pincers,[25] the exposure of the starting complex **1** to a H_2-rich (2/1 H_2/CO_2 mixture, 3 bar) at 70 °C in the presence of DBU (Figure 8a) does not result in the formate complex **4**, which is the resting state of the hydrogenolysis mechanism (Scheme 2).[26] Instead, in line with the theoretical predictions, under these conditions precatalyst **1** is quantitatively transformed to the CO_2 adducts **3**/**3b** with a concomitant formation of DBU-FA product of the catalytic reaction. The more thermodynamically stable complex **3** dominates the reaction mixture (Figure 8a). The [1,3]-addition of CO_2 is confirmed by the presence of only three methylene bridge protons, two of which appear as doublets at 5.81 and 5.29 ppm with J_{HH} = 13.5 Hz, while the remaining proton appears as sharp singlet at 6.12 ppm. The trans position of the hydride ligand with respect to the added CO_2 in **3** is evidenced by a significant high-field shift of the hydride resonance at −16.76 ppm. In line with the computational results, **3b** represents a minor species (approximately 12.7 mol %) in the reaction mixture. This isomer is characterized by similar spectral properties, except for the position of the hydride resonance that appears at −11.66 ppm (Figure 8), which is consistent with its position cis to the pyridine donor group (Scheme 3 and Figure 4).

Complexes **3**/**3b** are also readily formed in the absence of H_2 upon the exposure of **1** to CO_2 in the presence of DBU. The reaction mixture formed in this case exhibits an ^{1}H NMR spectrum (see the Supporting Information) similar to that characteristic for the catalytic reaction (Figure 8a). When labeled $^{13}CO_2$ is used to generate **3**/**3b**, the resonance of the single methylene proton shows J_{CH} = 5.3 Hz, typical for a two-bond C−H coupling. The same J_{CH} = 5.3 Hz is observed in ^{13}C

DOI: 10.1021/cs501990c
ACS Catal. 2015, 5, 1145−1154

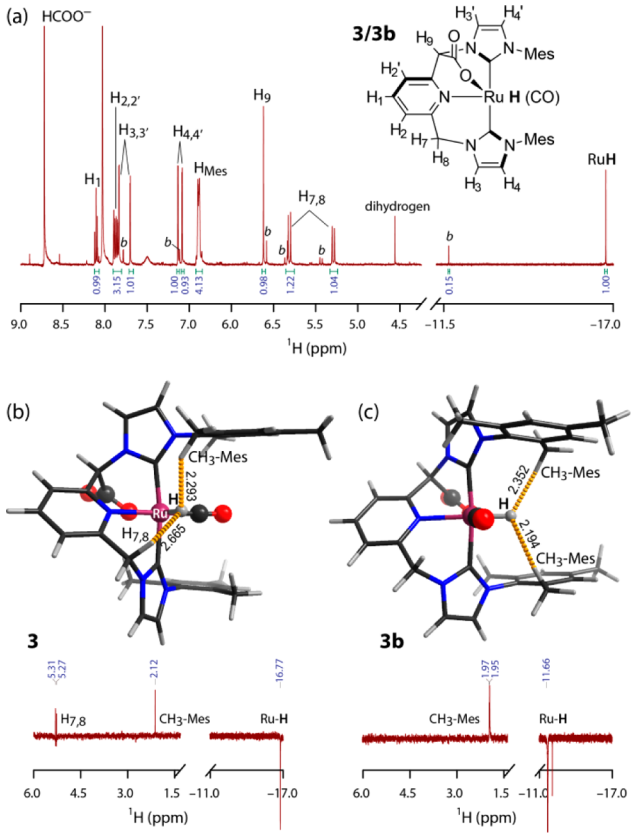

Figure 8. ^{1}H NMR spectrum (a) of the reaction mixture containing **1** and DBU in the presence of 3 bar of H_2/CO_2 (2/1) and DFT-optimized geometries and the DPFGSE 1D NOESY results for complexes (b) **3** and (c) **3b**, respectively.

NMR for doublets at 167.26 and 168.19 ppm corresponding to the metal−ligand bridging CO_2 moiety in **3** and **3b**, respectively. Finally, selective excitation NMR confirms the predicted structures of **3** and **3b** (Figure 8b,c). In agreement with the DFT-optimized geometries, the hydride signal at −16.77 ppm attributed to **3** shares a cross peak with a methylene bridge proton that appears as a doublet at 5.29 ppm and a singlet resonance of the CH_3-Mes group at 2.12 ppm (Figure 8b). On the other hand, the hydride resonance at −11.66 ppm correlates only with that of the CH_3-Mes groups (singlets at 1.97 and 1.95 ppm) located in the immediate vicinity of the hydride ligand in the DFT-optimized structure of **3b** (Figure 8c).

Complexes **3**/**3b** are stable at 70 °C in DMF/DBU mixtures for days. The CO_2 addition is irreversible under practical conditions. Vacuum treatment of the solutions of **3**/**3b** has no impact on the NMR spectrum. No detectable changes in the NMR spectrum are observed upon exposure of the solutions of **3**/**3b** to 3 bar of H_2, even on heating for several hours at 70 °C. These data confirm the theoretical predictions that **3** is highly stable under catalytically relevant conditions.

The formation of **3** accompanying the catalytic CO_2 hydrogenation results in the rapid deactivation of Ru−CNC catalyst. The maximum DBU conversion of 28% was reached under 40 bar of equimolar H_2/CO_2 (see the Supporting Information). This implies a complete deactivation of the catalytic system after 3200 turnovers. For comparison, the benchmark Ru−PNP system showed no sign of deactivation under similar conditions even when operated in the cyclic H_2 storage/release mode. This points to a manifold stronger inhibiting effect of the metal−ligand cooperative behavior of Ru−CNC in comparison to that of Ru−PNP.[25] Thus, to achieve a high and stable catalytic activity in the Ru−CNC system, the formation of **3** has to be suppressed and a high concentration of **2** has to be ensured under the catalytic conditions.

According to the results of ab initio thermodynamic analysis (Figure S2, Supporting Information), this can only be achieved in a very narrow window of conditions. In particular, **2** is the most thermodynamically stable complex in the catalytic system, operating at a low partial pressure of CO_2 (Figure S2). Indeed, the deactivated catalytic system discussed above can be reanimated by strongly decreasing the concentration of CO_2 in the gas phase (Figure S8, Supporting Information).

When the catalytic CO_2 hydrogenation with **1** is carried out at reduced CO_2 pressure (H_2/CO_2 = 39/1), the overall performance and the catalyst stability improve dramatically (Figure 9). At 84 °C catalyst **1** operates with an initial activities

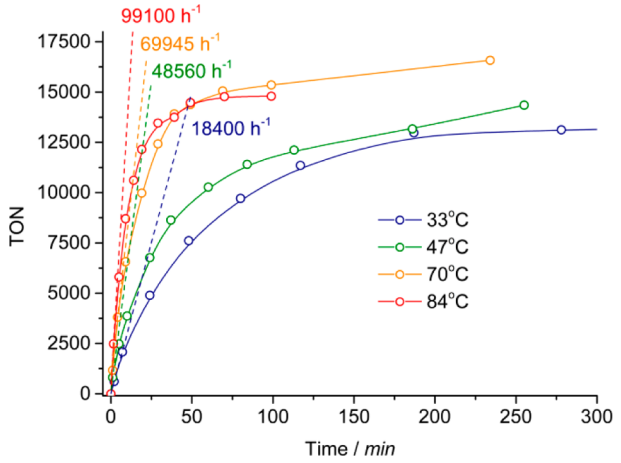

Figure 9. Kinetic traces for hydrogenation of CO_2 using **1** at different temperatures. Conditions: 39/1 H_2/CO_2 (bar/bar), 2.9 μmol of **1**, 30 mL of DMF, 5 mL of DBU (33.5 mmol).

(TOF°) of 99100 h^{-1}. The apparent activation energy (E_a) is 28 kJ mol^{-1}. This value is of the same order of magnitude as the DFT-computed overall barriers for the potential rate-determining steps of the hydrogenolysis mechanism,[26] namely **2**-CO_2 → $TS_{2\text{-}4}$ → **4*** ($E^{\ddagger}_{ZPE}$ = 13 kJ mol^{-1}) and **4** + H_2 → **4***+ H_2 → **4**-H_2 ($E^{\ddagger}_{ZPE}$ = 39 kJ mol^{-1}). Unfortunately, the complexity of the current reaction does not allow us to assign the rate-determining step in the same manner as we did earlier for Ru−PNP catalyzed CO_2 hydrogenation.[26] The direct consequence of such a low activation energy is the possibility to efficiently carry out the catalytic reaction at a low temperature. As an example, a very high catalytic activity of 18400 h^{-1} was attained already at 33 °C.

CONCLUSION

To summarize, we reported a mechanistic study of CO_2 hydrogenation catalyzed by cooperative Ru−CNC pincer catalyst **1**. Due to the strikingly different catalytic performance of **1** in comparison to that exhibited by the structurally related Ru−PNP complex, a special focus was given to the analysis of the reactivity of **1** and its potential impact on catalysis.

The activation of catalyst precursor **1** by a reaction with a strong base leads to the dearomatized Ru−CNC* complex **1***,

DOI: 10.1021/cs501990c
ACS Catal. 2015, 5, 1145−1154

which is highly reactive toward the ligand-assisted activation of H_2 and CO_2. In comparison to the analogous reactions with Ru−PNP pincer, the heterolytic H_2 cleavage and [1,4]-CO_2 addition to **1*** are more thermodynamically favorable and proceed with much lower barriers. The pronounced atropoisomization of Ru−CNC* results in two alternative mechanisms of CO_2 addition that yield the distinctly different CO_2 adducts **3** and **3b**.

The most important difference with the highly active Ru−PNP system is that the formation of the cooperative CO_2 adducts **3**/**3b** is much more thermodynamically favorable and proceeds with only a slightly higher free energy barrier than the reaction with H_2 toward the bis-hydrido Ru−CNC complex **2**, which is identified as the catalytically active species for CO_2 hydrogenation.

DFT calculations indicate a very high intrinsic activity of Ru−CNC. The favorable mechanism of the catalytic reaction with **2** does not involve metal−ligand cooperative transformations. The reaction in this case starts with nearly barrierless activation of CO_2 by Ru−H followed by a facile hydrogenolysis of the resulting formato species. The cycle is closed and the catalytic complex **2** is regenerated by neutralization of the coordinated FA with the DBU base. A competing path involves the deprotonation of the Ru−CNC intermediates that under the standard reaction conditions will rapidly convert to the CO_2 adducts **3**/**3b**, resulting in fast catalyst deactivation. In line with the in situ NMR observations, ab initio thermodynamic analysis predicts these complexes to represent the most stable species under a wide range of conditions. Theoretical calculations also indicate that the activity of Ru−CNC can be reanimated by carrying out the reaction under CO_2-poor conditions that will allow to shift the equilibrium toward the bis-hydrido complex **2**. Indeed, when the catalytic reaction is carried out at a H_2/CO_2 ratio of 39/1, Ru−CNC shows high and stable performance. The reaction proceeds with an apparent activation barrier of 28 kJ mol^{-1} that corresponds well with the barriers predicted by DFT calculations for the hydrogenolysis route over complex **2**.

This study illustrates the importance of a careful mechanistic analysis of the catalytic reactions which can provide optimal operation conditions and unleash the true potential of the catalytic system that could have been dismissed as inactive otherwise.

■ ASSOCIATED CONTENT

Supporting Information

The following file is available free of charge on the ACS Publications website at DOI: 10.1021/cs501990c.

Results of DFT calculations, optimized structures of all intermediates and transition states, results of ab initio thermodynamic analysis, in situ NMR spectroscopy, catalytic tests, and *xyz* coordinates of optimized structures (PDF)

■ AUTHOR INFORMATION

Corresponding Author

*E-mail for E.A.P.: e.a.pidko@tue.nl.

Author Contributions

⊥These authors contributed equally.

Notes

The authors declare no competing financial interest.

■ ACKNOWLEDGMENTS

E.A.P. thanks the Technology Foundation STW and The Netherlands Organization for Scientific Research (NWO) for his personal VENI grant. D.S. thanks the Polish Ministry of Science and Higher Education for a statutory activity subsidy (S405 62) for the Wrocław University of Technology cofinanced by the European Union within the European Social Fund. The computational work was partially performed using the computational resources of the Wrocław Center for Networking and Supercomputing and the Interdisciplinary Center for Mathematical and Computational Modeling. SurfSARA and NWO are acknowledged for providing access to supercomputer resources.

■ REFERENCES

(1) Centi, G.; Quadrelli, E. A.; Perathoner, S. *Energy Environ. Sci.* **2013**, *6*, 1711−1731.

(2) (a) Cokoja, M.; Bruckmeier, C.; Rieger, B.; Herrmann, W. A.; Kühn, F. E. *Angew. Chem., Int. Ed.* **2011**, *50*, 8510−8537. (b) Sakakura, T.; Choi, J.-C.; Yasuda, H. *Chem. Rev.* **2007**, *107*, 2365−2387.

(3) (a) Greenhalgh, M. D.; Thomas, S. P. *J. Am. Chem. Soc.* **2012**, *134*, 11900−11903. (b) Ohishi, T.; Zhang, L.; Nishiura, M.; Hou, Z. *Angew. Chem., Int. Ed.* **2011**, *50*, 8114−8117. (c) Lejkowski, M. L.; Lindner, R.; Kageyama, T.; Bódizs, G. É.; Plessow, P. N.; Müller, I. B.; Schäfer, A.; Rominger, F.; Hofmann, P.; Futter, C.; Schunk, S. A.; Limbach, M. *Chem.—Eur. J.* **2012**, *18*, 14017−14025. (d) Hendriksen, C.; Pidko, E. A.; Yang, G.; Schäffner, B.; Vogt, D. *Chem.—Eur. J.* **2014**, *20*, 12037−12040. (e) Yang, G.; Schäffner, B.; Blug, M.; Hensen, E. J. M.; Pidko, E. A. *ChemCatChem* **2014**, *6*, 800−807.

(4) Zhang, L.; Cheng, J.; Carry, B.; Hou, Z. *J. Am. Chem. Soc.* **2012**, *134*, 14314−14317.

(5) (a) Whiteoak, C. J.; Kielland, N.; Laserna, V.; Escudero-Adán, E. C.; Martin, E.; Kleij, A. W. *J. Am. Chem. Soc.* **2013**, *135*, 1228−1231. (b) Chatelet, B.; Joucla, L.; Dutasta, J.-P.; Martinez, A.; Szeto, K. C.; Dufaud, V. *J. Am. Chem. Soc.* **2013**, *135*, 5348−5351. (c) Sakai, T.; Tsutsumi, Y.; Ema, T. *Green Chem.* **2008**, *10*, 337−341.

(6) (a) Olah, G. A. *Angew. Chem., Int. Ed.* **2005**, *44*, 2636−2639. (b) Olah, G. A.; Prakash, G. K. S.; Goeppert, A. *J. Am. Chem. Soc.* **2011**, *133*, 12881−12898. (c) Wesselbaum, S.; vom Stein, T.; Klankermayer, J.; Leitner, W. *Angew. Chem., Int. Ed.* **2012**, *51*, 7499−7502. (d) Wesselbaum, S.; Moha, V.; Meuresch, M.; Brosinski, S.; Thenert, K. M.; Kothe, J.; vom Stein, T.; Englert, U.; Hoelscher, M.; Klankermayer, J.; Leitner, W. *Chem. Sci.* **2014**, *6*, 693.

(7) Williams, R.; Crandall, R. S.; Bloom, A. *Appl. Phys. Lett.* **1978**, *33*, 381−383.

(8) Joó, F. *ChemSusChem* **2008**, *1*, 805−808.

(9) (a) Boddien, A.; Gaertner, F.; Federsel, C.; Sponholz, P.; Mellmann, D.; Jackstell, R.; Junge, H.; Beller, M. *Angew. Chem., Int. Ed.* **2011**, *50*, 6411−6414. (b) Boddien, A.; Federsel, C.; Sponholz, P.; Mellmann, D.; Jackstell, R.; Junge, H.; Laurenczy, G.; Beller, M. *Energy Environ. Sci.* **2012**, *5*, 8907−8911.

(10) (a) Boddien, A.; Mellmann, D.; Gärtner, F.; Jackstell, R.; Junge, H.; Dyson, P. J.; Laurenczy, G.; Ludwig, R.; Beller, M. *Science* **2011**, *333*, 1733−1736. (b) Fellay, C.; Dyson, P. J.; Laurenczy, G. *Angew. Chem., Int. Ed.* **2008**, *47*, 3966−3968.

(11) Reutemann, W.; Kieczka, H. Formic Acid. In *Ullmann's Encyclopedia of Industrial Chemistry*; Wiley-VCH: Weinheim, Germany, 2000.

(12) (a) Schaub, T.; Paciello, R. A. *Angew. Chem., Int. Ed.* **2011**, *50*, 7278−7282. (b) Zhang, Z.; Hu, S.; Song, J.; Li, W.; Yang, G.; Han, B. *ChemSusChem* **2009**, *2*, 234−238.

(13) Bredig, G.; Carter, S. R. *Ber. Dtsch. Chem. Ges.* **1914**, *47*, 541−545.

(14) (a) Guyer, A.; Bieler, A.; Züger, E. *Helv. Chim. Acta* **1955**, *38*, 1308−1312. (b) Guyer, A.; Bieler, A.; Züger, E. *Helv. Chim. Acta* **1955**, *38*, 2027−2030.

DOI: 10.1021/cs501990c
ACS Catal. 2015, 5, 1145−1154

(15) (a) Jessop, P. G.; Ikariya, T.; Noyori, R. *Chem. Rev.* **1995**, *95*, 259−272. (b) Joó, F. *ChemCatChem* **2014**, DOI: 10.1002/cctc.201402591. (c) Schuchmann, K.; Müller, V. *Science* **2013**, *342*, 1382−1385.
(16) (a) Ziebart, C.; Federsel, C.; Anbarasan, P.; Jackstell, R.; Baumann, W.; Spannenberg, A.; Beller, M. *J. Am. Chem. Soc.* **2012**, *134*, 20701−20704. (b) Langer, R.; Diskin-Posner, Y.; Leitus, G.; Shimon, L. J. W.; Ben-David, Y.; Milstein, D. *Angew. Chem., Int. Ed.* **2011**, *50*, 9948−9952. (c) Federsel, C.; Boddien, A.; Jackstell, R.; Jennerjahn, R.; Dyson, P. J.; Scopelliti, R.; Laurenczy, G.; Beller, M. *Angew. Chem., Int. Ed.* **2010**, *49*, 9777−9780.
(17) Federsel, C.; Jackstell, R.; Beller, M. *Angew. Chem., Int. Ed.* **2010**, *49*, 6254−6257.
(18) Angermund, K.; Baumann, W.; Dinjus, E.; Fornika, R.; Görls, H.; Kessler, M.; Krüger, C.; Leitner, W.; Lutz, F. *Chem.—Eur. J.* **1997**, *3*, 755−764.
(19) (a) Himeda, Y.; Onozawa-Komatsuzaki, N.; Sugihara, H.; Kasuga, K. *Organometallics* **2007**, *26*, 702−712. (b) Tanaka, R.; Yamashita, M.; Nozaki, K. *J. Am. Chem. Soc.* **2009**, *131*, 14168−14169. (c) Tanaka, R.; Yamashita, M.; Chung, L. W.; Morokuma, K.; Nozaki, K. *Organometallics* **2011**, *30*, 6742−6750.
(20) (a) Jessop, P. G.; Hsiao, Y.; Ikariya, T.; Noyori, R. *J. Am. Chem. Soc.* **1996**, *118*, 344−355. (b) Munshi, P.; Main, A. D.; Linehan, J. C.; Tai, C.-C.; Jessop, P. G. *J. Am. Chem. Soc.* **2002**, *124*, 7963−7971. (c) Urakawa, A.; Jutz, F.; Laurenczy, G.; Baiker, A. *Chem. Eur. J.* **2007**, *13*, 3886−3899. (d) Huff, C. A.; Sanford, M. S. *ACS Catal.* **2013**, *3*, 2412−2416.
(21) (a) Gunanathan, C.; Milstein, D. *Acc. Chem. Res.* **2011**, *44*, 588−602. (b) Benito-Garagorri, D.; Kirchner, K. *Acc. Chem. Res.* **2008**, *41*, 201−213. (c) van der Vlugt, J. I.; Reek, J. N. H. *Angew. Chem., Int. Ed.* **2009**, *48*, 8832−8846. (d) Friedrich, A.; Drees, M.; Käss, M.; Herdtweck, E.; Schneider, S. *Inorg. Chem.* **2010**, *49*, 5482−5494. (e) Yang, X. *ACS Catal.* **2011**, *1*, 849−854. (f) Balaraman, E.; Gunanathan, C.; Zhang, J.; Shimon, L. J. W.; Milstein, D. *Nat. Chem.* **2011**, *3*, 609−614.
(22) Zhang, J.; Leitus, G.; Ben-David, Y.; Milstein, D. *Angew. Chem., Int. Ed.* **2006**, *45*, 1113−1115.
(23) Vogt, M.; Gargir, M.; Iron, M. A.; Diskin-Posner, Y.; Ben-David, Y.; Milstein, D. *Chem. Eur. J.* **2012**, *18*, 9194−9197.
(24) (a) Zhang, J.; Leitus, G.; Ben-David, Y.; Milstein, D. *J. Am. Chem. Soc.* **2005**, *127*, 10840−10841. (b) Huff, C. A.; Kampf, J. W.; Sanford, M. S. *Organometallics* **2012**, *31*, 4643−4645.
(25) Filonenko, G. A.; Conley, M. P.; Copéret, C.; Lutz, M.; Hensen, E. J. M.; Pidko, E. A. *ACS Catal.* **2013**, *3*, 2522−2526.
(26) Filonenko, G. A.; Hensen, E. J. M.; Pidko, E. A. *Catal. Sci. Technol.* **2014**, *4*, 3474−3485.
(27) (a) Hopkinson, M. N.; Richter, C.; Schedler, M.; Glorius, F. *Nature* **2014**, *510*, 485−496. (b) Nolan, S. P.; Clavier, H. *Chem. Soc. Rev.* **2010**, *39*, 3305−3316. (c) Velazquez, H. D.; Verpoort, F. *Chem. Soc. Rev.* **2012**, *41*, 7032−7060.
(28) Sun, Y.; Koehler, C.; Tan, R.; Annibale, V. T.; Song, D. *Chem. Commun.* **2011**, *47*, 8349−8351.
(29) (a) Hernandez-Juarez, M.; Vaquero, M.; Alvarez, E.; Salazar, V.; Suarez, A. *Dalton Trans.* **2013**, *42*, 351−354. (b) Filonenko, G. A.; Cosimi, E.; Lefort, L.; Conley, M. P.; Coperet, C.; Lutz, M.; Hensen, E. J. M.; Pidko, E. A. *ACS Catal.* **2014**, *4*, 2667−2671.
(30) Adamo, C.; Barone, V. *J. Chem. Phys.* **1999**, *110*, 6158−6170.
(31) Frisch, M. J.; Trucks, G. W.; Schlegel, H. B.; Scuseria, G. E.; Robb, M. A.; Cheeseman, J. R.; Scalmani, G.; Barone, V.; Mennucci, B.; Petersson, G. A.; Nakatsuji, H.; Caricato, M.; Li, X.; Hratchian, H. P.; Izmaylov, A. F.; Bloino, J.; Zheng, G.; Sonnenberg, J. L.; Hada, M.; Ehara, M.; Toyota, K.; Fukuda, R.; Hasegawa, J.; Ishida, M.; Nakajima, T.; Honda, Y.; Kitao, O.; Nakai, H.; Vreven, T.; Montgomery, J. A., Jr.; Peralta, J. E.; Ogliaro, F.; Bearpark, M.; Heyd, J. J.; Brothers, E.; Kudin, K. N.; Staroverov, V. N.; Kobayashi, R.; Normand, J.; Raghavachari, K.; Rendell, A.; Burant, J. C.; Iyengar, S. S.; Tomasi, J.; Cossi, M.; Rega, N.; Millam, N. J.; Klene, M.; Knox, J. E.; Cross, J. B.; Bakken, V.; Adamo, C.; Jaramillo, J.; Gomperts, R.; Stratmann, R. E.; Yazyev, O.; Austin, A. J.; Cammi, R.; Pomelli, C.; Ochterski, J. W.; Martin, R. L.; Morokuma, K.; Zakrzewski, V. G.; Voth, G. A.; Salvador, P.; Dannenberg, J. J.; Dapprich, S.; Daniels, A. D.; Farkas, Ö.; Foresman, J. B.; Ortiz, J. V.; Cioslowski, J.; Fox, D. J. *Gaussian 09, Revision D.01*; Gaussian, Inc., Wallingford, CT, 2009.
(32) Li, G.; Pidko, E. A.; van Santen, R. A.; Li, C.; Hensen, E. J. M. *J. Phys. Chem. C* **2013**, *117*, 413−426.
(33) (a) Zhao, Y.; Truhlar, D. G. *J. Chem. Theory Comput.* **2009**, *5*, 324−333. (b) Valero, R.; Costa, R.; de P. R. Moreira, I.; Truhlar, D. G.; Illas, F. *J. Chem. Phys.* **2008**, *128*, 114103.
(34) Müller, C.; Pidko, E. A.; Staring, A. J. P. M.; Lutz, M.; Spek, A. L.; van Santen, R. A.; Vogt, D. *Chem. Eur. J.* **2008**, *14*, 4899−4905.

DOI: 10.1021/cs501990c
ACS Catal. 2015, 5, 1145−1154